Biomaterials 63 (2015) 24–34

Contents lists available at ScienceDirect

Biomaterials

journal homepage: www.elsevier.com/locate/biomaterials

Ex vivo engineered immune organoids for controlled germinal center reactions

Alberto Purwada [a], Manish K. Jaiswal [b], Haelee Ahn [c], Takuya Nojima [d], Daisuke Kitamura [d], Akhilesh K. Gaharwar [b, e], Leandro Cerchietti [c], Ankur Singh [f, *]

[a] Department of Biomedical Engineering, Cornell University, Ithaca, NY 14853, USA
[b] Department of Biomedical Engineering, Texas A&M University, College Station, TX 77843, USA
[c] Division of Hematology and Medical Oncology, Weill Cornell Medical College of Cornell University, New York, NY 10065, USA
[d] Division of Molecular Biology, Research Institute for Biomedical Sciences (RIBS), Tokyo University of Science, Noda, Chiba 278-0022, Japan
[e] Department of Materials Science & Engineering, Texas A&M University, College Station, TX 77843, USA
[f] Sibley School of Mechanical and Aerospace Engineering, Cornell University, Ithaca, NY 14853, USA

ARTICLE INFO

Article history:
Received 31 May 2015
Accepted 1 June 2015
Available online 3 June 2015

Keywords:
B cell
Germinal center
Nanocomposite biomaterials
Immuno-engineering
Organoids
Class switching

ABSTRACT

Ex vivo engineered three-dimensional organotypic cultures have enabled the real-time study and control of biological functioning of mammalian tissues. Organs of broad interest where its architectural, cellular, and molecular complexity has prevented progress in *ex vivo* engineering are the secondary immune organs. *Ex vivo* immune organs can enable mechanistic understanding of the immune system and more importantly, accelerate the translation of immunotherapies as well as a deeper understanding of the mechanisms that lead to their malignant transformation into a variety of B and T cell malignancies. However, till date, no modular *ex vivo* immune organ has been developed with an ability to control the rate of immune reaction through tunable design parameter. Here we describe a B cell follicle organoid made of nanocomposite biomaterials, which recapitulates the anatomical microenvironment of a lymphoid tissue that provides the basis to induce an accelerated germinal center (GC) reaction by continuously providing extracellular matrix (ECM) and cell–cell signals to naïve B cells. Compared to existing co-cultures, immune organoids provide a control over primary B cell proliferation with ~100-fold higher and rapid differentiation to the GC phenotype with robust antibody class switching.

1. Introduction

Secondary immune organs, such as lymph node, tonsil and spleen, are highly structured tissues which dynamically change mechanical and biological functionality in response to antigens [1–4]. Of particular importance is the activation of naïve B cells in these lymphoid tissues to form sub-anatomical structures, germinal center (GC), that program B cell conversion into antibody producing cells [5,6], which represents a powerful defense mechanism against pathogens and is characterized by immunological memory. To date, we have relied heavily on live animal models to understand immune cell development, functioning, and screening of immunotherapies against diseases [7], but such approaches are costly with long turnaround times. We are yet to fully understand how the cell microenvironment in lymphoid organs facilitates the GC reaction that leads to the production of antibodies [2,8,9]. Therefore, *ex vivo* engineered B cell organoids could offer a new approach for studying GC B cell physiology and pathology [10–15], and potentially hematological malignancies of B cell origin [11,15–24], as well as screening of therapeutics including immunotherapeutics [7,15,23–28].

From an anatomical perspective, secondary lymphoid organs are composed of supporting cellular compartments, including B and T cells, that work together to orchestrate adaptive immune responses [8,9,29]. B cell follicles are composed of a dense stromal network of B cell activating follicular dendritic cells (FDCs) [30,31] and Arg-Gly-Asp (RGD)-presenting ECM [32]. Activation process requires interactions between antigen-primed B cells and follicular helper T (T_{FH}) cells via a CD40L ligand, and secretion of IL-4 [31]. GC B cells are naturally prone to apoptosis unless rescued by anti-apoptotic signals [12,33,34]. Although activation of B cells can be achieved through stimulation with antibodies (anti-Ig or anti-CD40), CD40L,

* Corresponding author.
E-mail address: as2833@cornell.edu (A. Singh).

http://dx.doi.org/10.1016/j.biomaterials.2015.06.002
0142-9612/

lipopolysaccharide and cytokines, such as IL-4, *in vitro*, the resulting cell growth is transient with poor cell survival and these works have not investigated the GC reaction in the context of lymphoid tissue microenvironment and have not shown the ability to modulate the extent of GC reaction [35–38]. Previous studies have demonstrated the combination of 3D scaffold and engineered stromal cell lines for generating artificial secondary lymphoid organs, however these scaffolds have shown GC formation when implanted *in vivo* by exploiting the host microenvironment [39,40]. In addition, recent studies have emphasized that interactions between B cells and RGD domain from the ECM component of lymphoid organs could promote long-term cell survival [32] and the RGD-binding integrin αvβ3 is up-regulated in GC B cells enabling GC fitness [41].

To bridge the functional gap between *in vivo* and *in vitro* systems, we have developed a biomaterials-based platform to engineer B cell follicles *ex vivo* by integrating known structural and signaling components of lymphoid microenvironment to recapitulate key functional events prior to GC formation. We engineered an RGD-presenting hydrogel scaffold reinforced with silicate nanoparticles (SiNP) as an immune organoid consisting of primary naïve B cells co-cultured with stromal cells that simultaneously present T_{FH} specific CD40L and B cell activating factor (BAFF) and supplemented the culture with IL-4. We hypothesized that combination of 3D ECM structural property, adhesive ligand, and stromal network with key signaling molecules would lead to faster development and differentiation of primary naïve B cells into GC phenotype and allow us to precisely control the magnitude and rate of GC reaction.

2. Materials and methods

2.1. Naïve B cell isolation and engineered stromal cells

For examining GC formation *in vivo*, C57BL6 mice were challenged with the T cell dependent antigen sheep red blood cells at 2% (Cocalico Biologicals, Inc). After 10 days, spleens were harvested to examine B cell follicles for the evidence of GC formation using immunohistochemistry (IHC), flow cytometry and immunofluorescence. IHC of paraffin-embedded serial spleen sections from mice were stained with CD45R/B220 (BD Pharmigen) for B cells and biotinylated peanut agglutinin (PNA, Vector Laboratories) for GC B cells as previously reported by us [42]. For flow cytometry, splenocytes were isolated by a combination of mechanical and gradient separation methods (Fico/Lite-LM, Atlanta Biologicals) and stained with CD45R/B220 for B cells and GL7 and Fas (BD Pharmigen) for GC B cells. In these studies, CD45R/B220 was used for visualizing B cells throughout the lymphoid tissue. This B220 population may contain CD19- population that induces follicular dendritic cell network formation as well as GC forming CD19+ cells [43,44]. For germinal center phenotype, CD19+ B cell population was further analyzed for two conventional GC markers: GL7 and Fas. For organoid experiments, spleens were freshly obtained from C57BL6 mice as per institutional guidelines. B cells were obtained from splenocytes through negative selection using EasySep™ Mouse B cell Isolation Kit (Stem Cell Technologies) in accordance with manufacturer's protocol (yield ~ 90% CD19+). The 40LB cells, that express CD40L and produce BAFF, were generated as reported earlier by us [45] and cultured in DMEM media (Life Technologies) with 10% FBS and 1% P/S. The 40LB cells were mitotically inhibited through incubation in cell culture medium containing 0.01 mg/mL Mitomycin C at 37 °C for 45 min in complete media conditions prior to the encapsulation. The cells were rinsed twice with 10 mL of 1× PBS before usage in the experiments.

2.2. Immune organoid fabrication

Gelatin stock solution was freshly prepared by mixing gelatin powder (Sigma Aldrich) in RPMI 1640 medium followed by sterilization using syringe filter. Cells were mixed with warmed gelatin stock solution and diluted accordingly using cell culture medium. SiNP with 25–30 nm in diameter and 1 nm in thickness were obtained from Southern Clay Products Inc., USA. SiNP suspension was freshly prepared prior to the encapsulation procedure by mixing SiNP powder with deionized water and vortexing the resulting solution, followed by filtration through 0.22 μm syringe filters immediately before use. Organoids were fabricated in 96-well plates by first adding 5 μL of SiNP followed by injecting 5 μL cell-containing gelatin solution into the initial SiNP droplet, and then mixing the entire hydrogel through repeated pipetting. Each organoid was cured for approximately 10 min prior to the addition of RPMI 1640 medium. Following the completion of fabrication steps, the entire plate was placed in cell culture incubator for 1 h before replacing cell culture medium in each well with that containing 100 ng/mL murine recombinant IL-4 (Peprotech). IL-4 stock solution was reconstituted in deionized water at 0.1 mg/mL concentration and kept as aliquots in −20 °C. The medium was replaced every 3 days.

2.3. Material characterizations

Gelatin solutions of 2 and 4% (weight %) were prepared in PBS, mixed and vortexed with aqueous suspensions of SiNPs to obtain homogeneously cross-linked gels. All the modulus measurements were carried out for strain sweep (1–10% strain) at a fixed frequency of 0.1 Hz, at 37 °C using a rheometer (Anton Paar) equipped with 50 mm flat-plate geometry and a gap of 50 μm. For scanning electron microscopy (SEM), samples were freeze dried and sliced into transverse sections by razor slitting. The sections were then sputter coated with Pt/Pd to provide conductivity. All the images were captured using Quanta 600 (FEI) at 20 kV equipped with energy-dispersive X-ray spectroscopy (EDS) detector (Oxford Instruments). The recorded EDS spectra were further analyzed by INCA software (Oxford Instruments) to confirm the presence of elements. For transmission electron microscopy (TEM) imaging of the SiNPs, approximately 5 μL volume of SiNPs in water was drop-casted onto a carbon-coated copper grid and air-dried. The images were captured under 200 keV voltage using JEOL JEM-2010 instrument (Japan). Bacterial endotoxin studies were performed using the US Food and Drug Administration (FDA) guidelines using limulus amebocyte lysate (LAL) assay [46].

2.4. Cell extraction from organoids

Cell culture media was aspirated from each well. The organoid was washed once using 1× PBS and then incubated overnight in 10 U/mL collagenase solution (Worthington Biosciences) in cell culture conditions. The collagenase solution was prepared by reconstituting collagenase powder in serum-free RPMI 1640 medium. Following incubation, the organoid was disintegrated through pipetting and diluted in FACS buffer (1× PBS +/+ with 10% FBS) for collagenase inactivation. The resulting cell suspension was passed through a 70 μm cell strainer to remove gel debris prior to flow cytometry analysis.

2.5. Immunofluorescence microscopy and flow cytometry analysis

Immune organoids were rinsed and incubated in FACS buffer containing fluorescence-conjugated antibodies and/or live cell stains for 12 h in cell culture conditions. The samples were washed

three times with each wash involving the aspiration of old medium and incubation in fresh FACS buffer for 1 h. Each organoid was covered with 1× PBS during imaging with Zeiss 710 confocal microscope (Zeiss). In all flow cytometry experiments, we started with same number of naïve B cells, i.e. 20,000 B cells. At each time point, samples were degraded using collagenase and the entire cell suspension (regardless of the final cell numbers) was re-suspended in equal volume for all samples and equally divided into 3 separate staining groups for flow cytometry analysis (to stain for CD19, GL7, Fas, IgM, IgG1, and IgE). The entire volume was analyzed for total number of cells. Extracted cells were stained by incubation in FACS buffer containing various combinations of antibodies with 1:1000 dilution for 45 min in the dark at 4 °C. The antibodies consisted of: FITC-, APC, or PE-Cy7-conjugated anti-mouse CD19, GL7, Fas, CD40L, IgG, and IgM (eBioscience). FACS buffer was prepared using 1× PBS ++ with 10% FBS. The cell suspension was rinsed twice using the same buffer prior to low cytometer using BD Accuri™ C6 flow cytometer. Data analysis was performed using FlowJo (Tree Star).

2.6. RGD blocking

B cells were incubated in FACS buffer containing integrin inhibitor at specific concentrations for 30 min at 4 °C. The buffer was prepared from 1× PBS and 10% FBS. In this experiment, cyclic RGD peptide (Cilengitide) was used with a final concentration of 10 or 50 μM in the blocking solution.

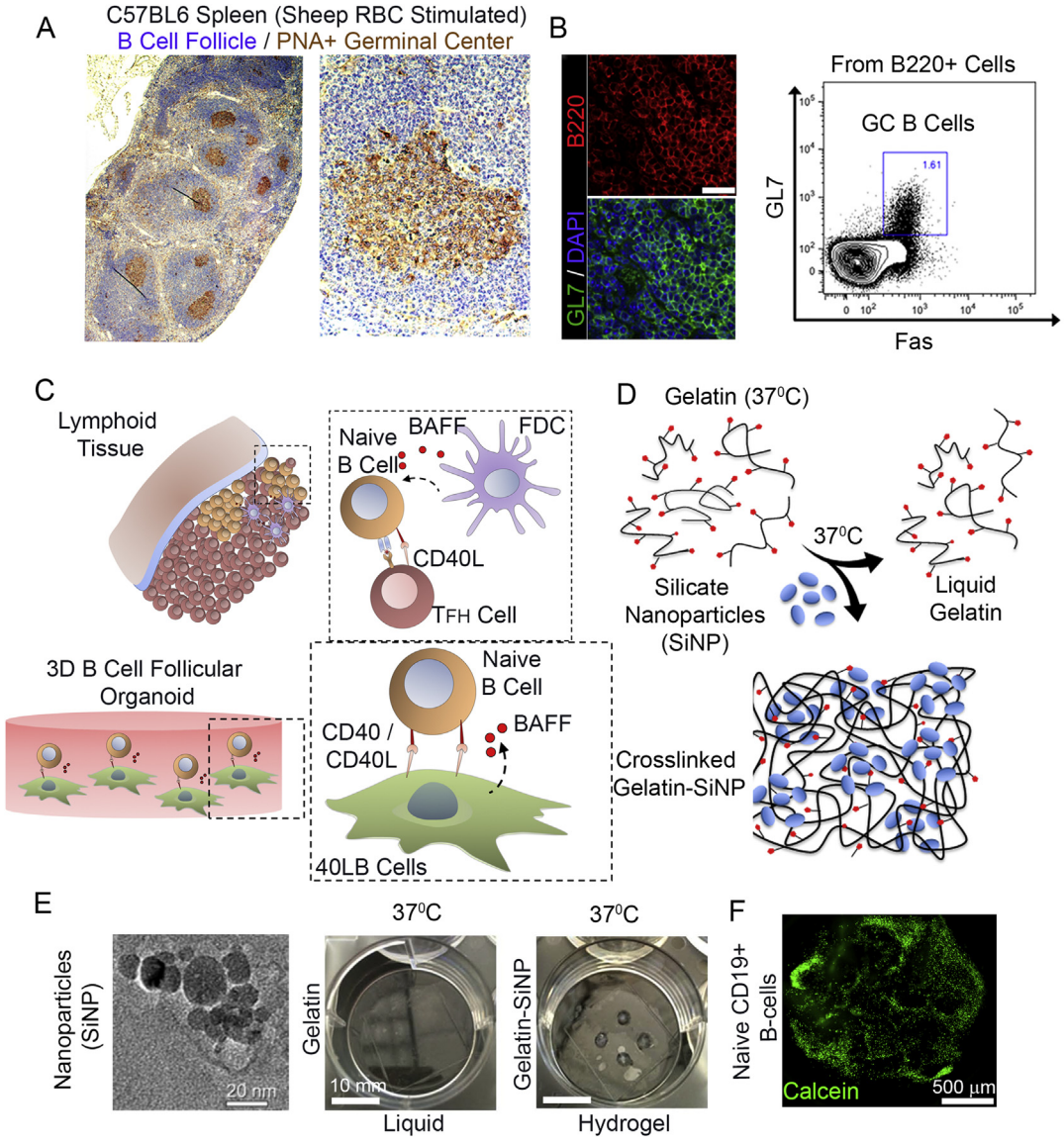

Fig. 1. *Ex vivo* engineered B cell follicle organoid. (A) Immunohistochemical analysis of a spleen stained for H&E and GC marker peanut agglutinin (PNA). Right panel represents immunofluorecnece images of splenic tissue stained with GC marker GL7; scale bar 50 μm. (B) Flow cytometry analysis of B220+ primary B cells from immunized C57BL6 mice with the gate indicating GL7+Fas+ GC B cell population. (C) Schematic of the *in vivo* interaction between mature naïve B cells with follicular T helper (T_{FH}) cells and follicular dendritic cells (FDCs) within the lymphoid tissue follicle. FDCs produce B cell activation factor (BAFF) that support naïve B cell activation and conversion to germinal center phenotype. (D) Overview on the use of silicate nanoparticles (SiNP) for ionic crosslinking of gelatin to form stable hydrogel at 37 °C. (E) TEM of silicate nanoparticles (Left, scale bar 20 nm). Hydrogels composed of gelatin only and those ionically cross-linked with SiNP were compared for gelation at 37 °C (Right, scale bar 10 mm). (F) Primary B cell viability and distribution 24 h following the encapsulation procedure (Bottom; green: Calcein; scale bar 500 μm). (For interpretation of the references to colour in this figure legend, the reader is referred to the web version of this article.)

2.7. Statistical analysis

Analysis of variance (ANOVA) statistical analyses were performed using GraphPad Prism software with Tukey's test (1-way ANOVA) or Bonferroni correction (2-way ANOVA). A p-value of less than 0.05 was considered significant. Two tail t-test was performed for RGD inhibition analysis. All studies were performed in triplicates unless otherwise noted. All values are reported as Mean ± S.E.M.

3. Results

3.1. Ex vivo engineered B cell follicle organoid

We first examined the structural organization of a secondary lymphoid organ by challenging C57BL6 mice with the T cell dependent antigen sheep red blood cell and examined the B cell follicle and GC formation. Activated B cells in primary follicles proliferated rapidly to form GCs expressing Fas (tumor necrosis factor receptor superfamily member 6) and GL7 surface markers (Fig. 1A, B). Reconstructing from this model and the existing knowledge of dependency of lymphoid B cells on T cell-mediated CD40L and FDC-mediated BAFF signaling [5,31], BALB/c 3T3 fibroblasts were stably transfected with both CD40L and BAFF (called hereafter 40LB), as reported earlier by Nojima et al. [45] (Fig. 1C). Primary B cells with 40LB stromal cells were co-encapsulated into an RGD-presenting nanocomposite hydrogel of gelatin ionically cross-linked with SiNP that were 20–30 nm in diameter and ~1 nm in thickness (Fig. 1D, E). While gelatin-based 3D hydrogels have existed for decades, mostly as chemically modified system that require UV exposure (methacrylate functionalities [47]), we have engineered hydrogels of polyampholytic gelatin that ionically interacts with the anisotropically distributed opposite charges on the synthetic SiNP resulting in hydrogels [48–50] that remain stable and do not liquefy at 37 °C (Fig. 1E). Primary B cells were successfully encapsulated in these hydrogels and stained positive for Calcein after 24 h of encapsulation (Fig. 1F).

3.2. Organoid material properties regulate the spreading and functional behavior of engineered stromal 40LB cells

An important criterion for material selection was the structural resemblance to the microarchitecture of compartments in the lymphoid tissue [51], which provides structural stability and yet allow for cell proliferation and dense stromal network formation (Fig. 1A). Using SEM, we evaluated the effect of SiNP concentration on hydrogel microarchitecture (Fig. 2A). Hydrogels with 2% gelatin and 1.5% SiNP resulted in more uniformly distributed porous structure in comparison to gelatin-only mixture, which could be attributed to the presence of charged surface in SiNP that would prevent the ionic aggregation of gelatin fibers with each other (zeta potential − 28 ± 3 mV vs. 4 ± 0.4 mV, respectively). This observation is further supported by the marked decrease in pore size as gelatin concentration was raised from 2% to 4% while keeping SiNP concentration constant at 1.5%. The presence of SiNP in hydrogels was confirmed with EDS analysis [50] that indicated the presence of Mg

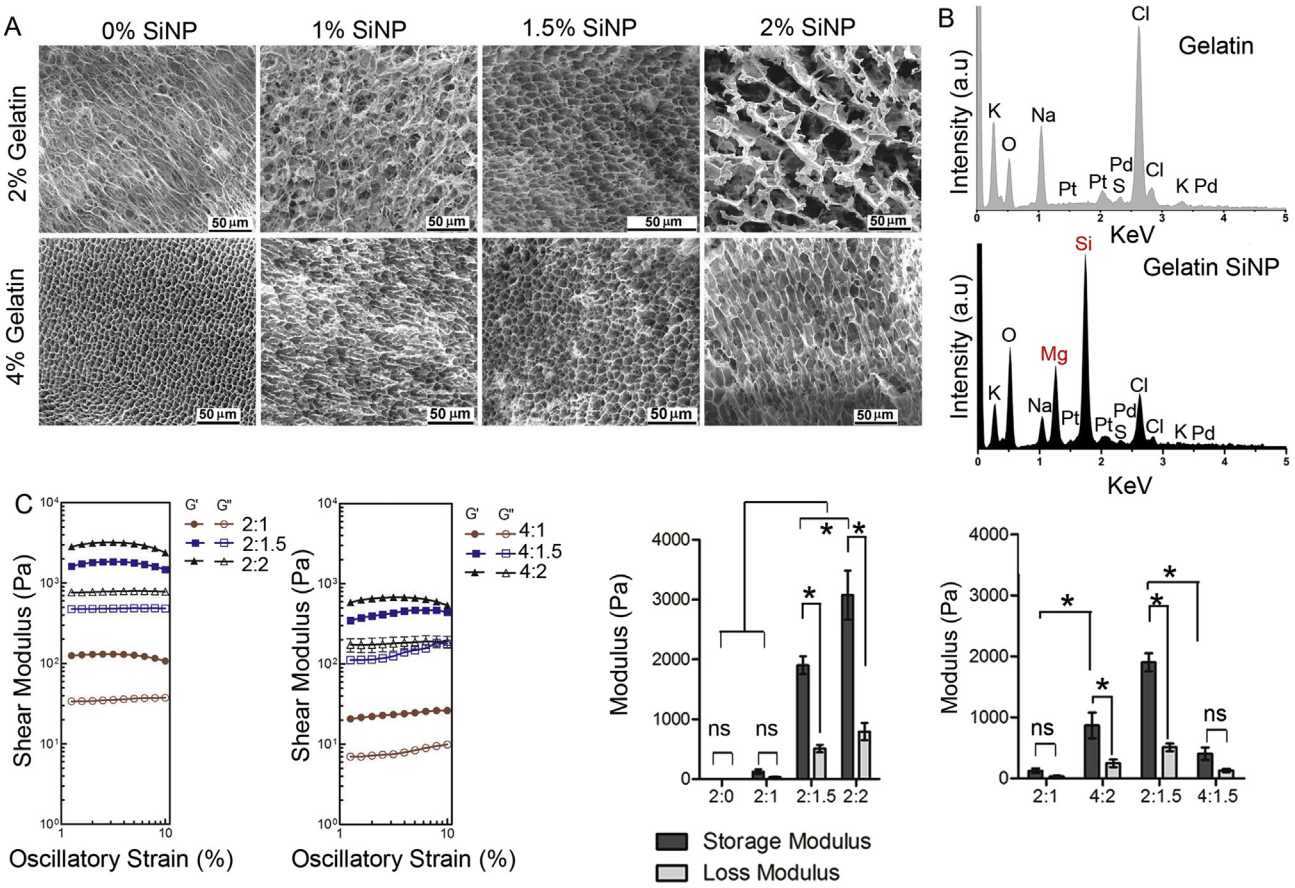

Fig. 2. Material characterization of immune organoids. (A) SEM analysis of hydrogel compositions with 2% and 4% gelatin with and without SiNP. (B) Energy-dispersive X-ray spectroscopy analysis in gelatin hydrogel with and without SiNP. (C) Rheological analysis on storage and loss moduli for 2% gelatin hydrogel with or without SiNP weight %. Mean ± S.E.M, n = 5, *P < 0.05, ANOVA with post-hoc Tukey's test.

and Si peak only in SiNP cross-linked hydrogels but not in plain gelatin gels (Fig. 2B).

We hypothesized that for an immune organoid to be functional, the material stiffness should be in close proximity to the reported stiffness of secondary lymphoid organs (2300 ± 1000 Pa) [52]. We determined the storage and loss modulus of hydrogels under physiological conditions (pH 7.4 and 37 °C) where gelatin remained liquid with no detectable storage and loss moduli, but the addition of SiNP resulted in a cross-linked gelatin network increasing the organoid stiffness. As indicated in Fig. 2C, the storage modulus of the cross-linked network increased marginally to 130 ± 40 Pa with the incorporation of 1% SiNP ($p > 0.05$), however increased significantly to 1900 ± 50 Pa with 1.5% SiNP incorporation ($p < 0.001$), which is closer to the stiffness (storage modulus) of lymphoid tissues. Further increase in SiNP concentration to 2.0% resulted in substantial increase in hydrogel stiffness to 3100 ± 410 Pa ($p < 0.001$). Importantly, the 2% gelatin hydrogel with 1% SiNP was fragile, which can be explained by a non-significant difference in storage and loss moduli ($p > 0.05$). Using the same weight ratio (i.e. 2:1), 4% gelatin with 2% SiNP resulted in significant differences between G′ and G″ making the hydrogel stable ($p < 0.05$). Interestingly, with the same SiNP weight percent, increase in gelatin weight percent from 2 to 4 % resulted in an instable hydrogel network, which could be attributed to the excess uncross-linked gelatin. This observation is further supported by the low storage modulus at 4% gelatin with 1.5% SiNP, with no significant differences between G′ and G″ ($p > 0.05$).

To assess the influence of material composition toward network formation of 40LB cells, we encapsulated CellTracker™ Green CMFDA stained 40LBs at 40,000 cells per hydrogel with increasing amount of gelatin or SiNP (Fig. 3A). By keeping the adhesive ligand density same (i.e. 2% gelatin), 40LBs demonstrated markedly more spreading with 1.5% SiNP than with 2% SiNP. Increase in adhesive ligand density to 4% gelatin resulted in marked clustering (Fig. 3A). We next examined the effect of seeding density of 40LB stromal cells within 2% gelatin hydrogels with 1.5% SiNP. As indicated in Fig. 3B, 20,000 seeding density formed small clusters over 48 h whereas 40,000 cell seeding density resulted in tightly connected cellular network, and 60,000 cells formed a dense tubular-like network. These results clearly indicate that 2% gelatin with 1.5% SiNP present a stable hydrogel network that permits uniform cell spreading as a function of stromal cell density. Importantly, 3D encapsulation of 40LBs in these hydrogels resulted in a significantly higher ($p < 0.001$) expression of CD40L surface marker compared to 2D cultures by day 6 of culture (mean fluorescent intensity 9500 ± 430 AU for 3D cultured 40LB versus 4600 ± 620 AU for 2D cultured 40LBs on tissue culture plastic surface), emphasizing the importance of 3D follicular niche (Fig. 3C). CD40L expression for 40LBs cultured in 3D was comparable to that observed with cells on day 0 (9500 ± 150 AU). These observations clearly indicate that 2% gelatin with 1.5% SiNP had the most favorable 40LB response and supports our hypothesis that optimal stromal cell functioning is observed at hydrogel stiffness mimicking that of the native secondary lymphoid tissue.

3.3. *Ex vivo proliferation of primary B cells within the immune organoid and role of integrins*

Based on our observation of the dependency of 40LB cells on the biophysical characteristics and cellular compositions of the hydrogels, we expected the interaction between cells and the 40LB

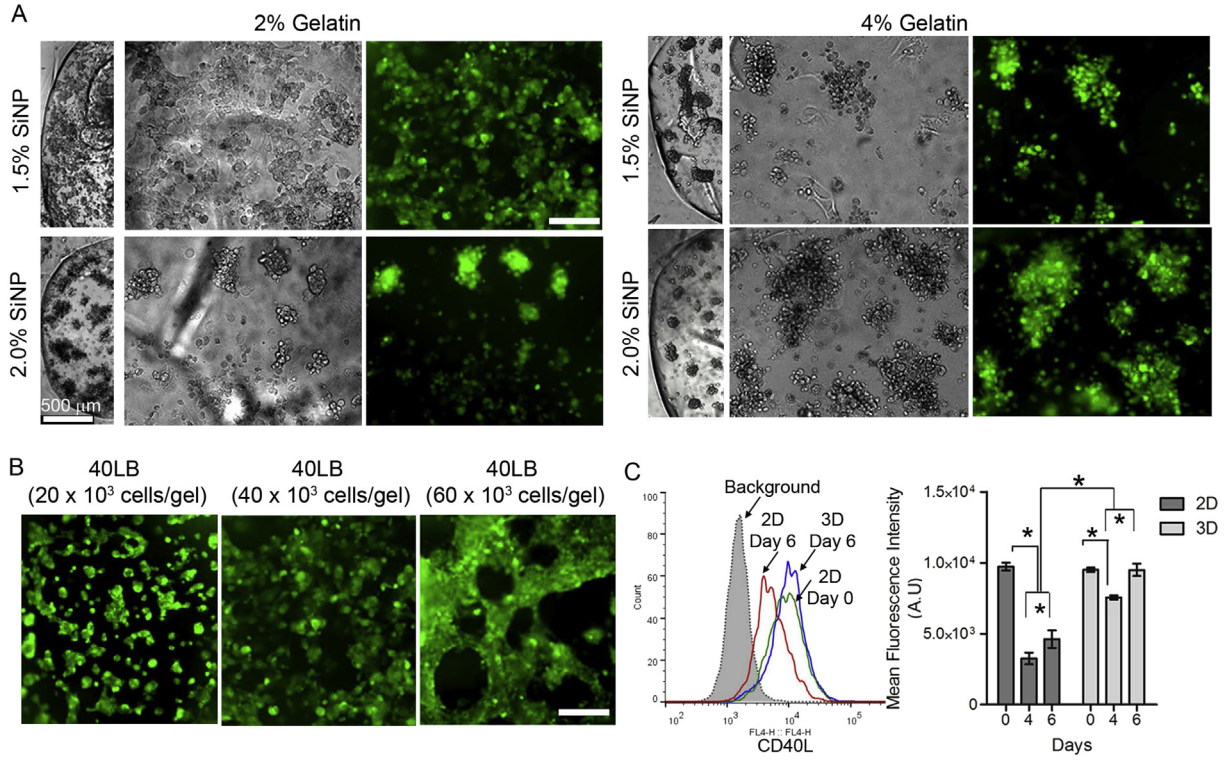

Fig. 3. Organoid stiffness affects 40LB stromal network and CD40L expression. (A) Fluorescence images of the 40LB stromal cell network formation with concentrations of gelatin and SiNP at 40,000 cells. Scale bar 200 μm (B) Fluorescence images of the 40LB stromal cell network formation with 2% gelatin and 1.5% SiNP and varying 40LB seeding density. Scale bar 200 μm (C) Histogram representing the overlay of CD40L expression for 2D culture of 40LBs on tissue culture plates versus 3D encapsulation in 2% gelatin with 1.5% SiNP organoids (Left). Bar graph representing mean fluorescence intensity of CD40L ligand expression in 2D and 3D cultures of 40LB (Right, Mean ± S.E.M, n = 4). *P < 0.05, 2-way ANOVA with post-hoc Bonferroni correction.

network to depend on stromal cell density. We next performed co-cultures of naïve B cells with 40LBs as a function of 40LB density in presence of 100 ng/mL IL-4. As indicated in Fig. 4A, we observed distinct regions of closely packed cells in hydrogels that morphologically resembled the proliferating GC inside the B cell follicles (Fig. 1A). Importantly, this morphological appearance was a function of 40LB density and qualitatively indicated B cell follicle formation and high proliferation of B cells in the organoids, as observed in GC reactions *in vivo*. We next evaluated the total number of live cells using flow cytometry (Calcein+, Fig. 4B) and observed a significant increase in the number of viable cells over 4 days in our 3D organoids in comparison to 2D systems when B cells were co-cultured with 40LB in media supplemented with 100 ng/mL IL-4 ($p < 0.05$).

We next performed 2D co-culture analysis for CD19+ B cells at 20,000, 40,000, and 60,000 40LB cells. Each condition consisted of 20,000 naïve B cells and at the completion of study, the harvested cells were equally divided into 3 groups for further analysis. As indicated in Fig. 4C, the total number of CD19+ cells was significantly reduced in 2D cultures and there was no significant difference between any of the 40LB seeding densities. Therefore, 20,000 40LB cell seeding density was considered for further comparison. We determined the role of cell seeding density in 3D organoids and noted that the presence of 40,000 40LB cells in hydrogels resulted in maximum proliferation of CD19+ B cells over 4 days compared with other seeding densities within the 3D groups (Day 0: Naïve B cells 6500 cells; Day 4: 3D B+40LB with 40,000 40LBs resulted in 5477 ± 477 cells versus 3D B+40LB with 20,000 40LBs resulted in 3390 ± 295 cells and 2D B+40LB with 20,000 40LBs resulted in with 1261 ± 72 cells; Fig. 4D and Supplementary Fig. S1). These findings indicate that the efficient stromal spreading and CD40L ligand interactions triggered the proliferation of CD19+ B cells. We evaluated the survival of CD19+ B cells after 2 days of culture in the organoids without any stromal support and observed a significant decrease in CD19+ B cell numbers in 2D co-culture compared to 3D B cell only cultures (Fig. 4E). Since gelatin has abundant RGD motifs, which are the cell attachment sites recognized by many integrins [53] and lymphoid B cells bind to RGD domains [32,41], we blocked the RGD-mediated signaling using Cilengitide, a cyclic RGD pentapeptide that selectively inhibits αvβ3 and αvβ5 integrin binding to RGD [54,55]. As indicated in Fig. 4F, we observed a partial but significant decrease in CD19+ B cells when blocked with Cilengitide, which at least confirmed the partial role of αvβ3 and αvβ5 integrins in supporting B cell survival in the organoids.

3.4. Ex vivo induction into GC reaction within the immune organoid

Importantly, of these CD19+ cells, the organoid culture with B+40LB at 40,000 and 60,000 40LBs induced ~100-fold increase in GC-specific marker GL7 within 4 days compared to a 10–20-fold

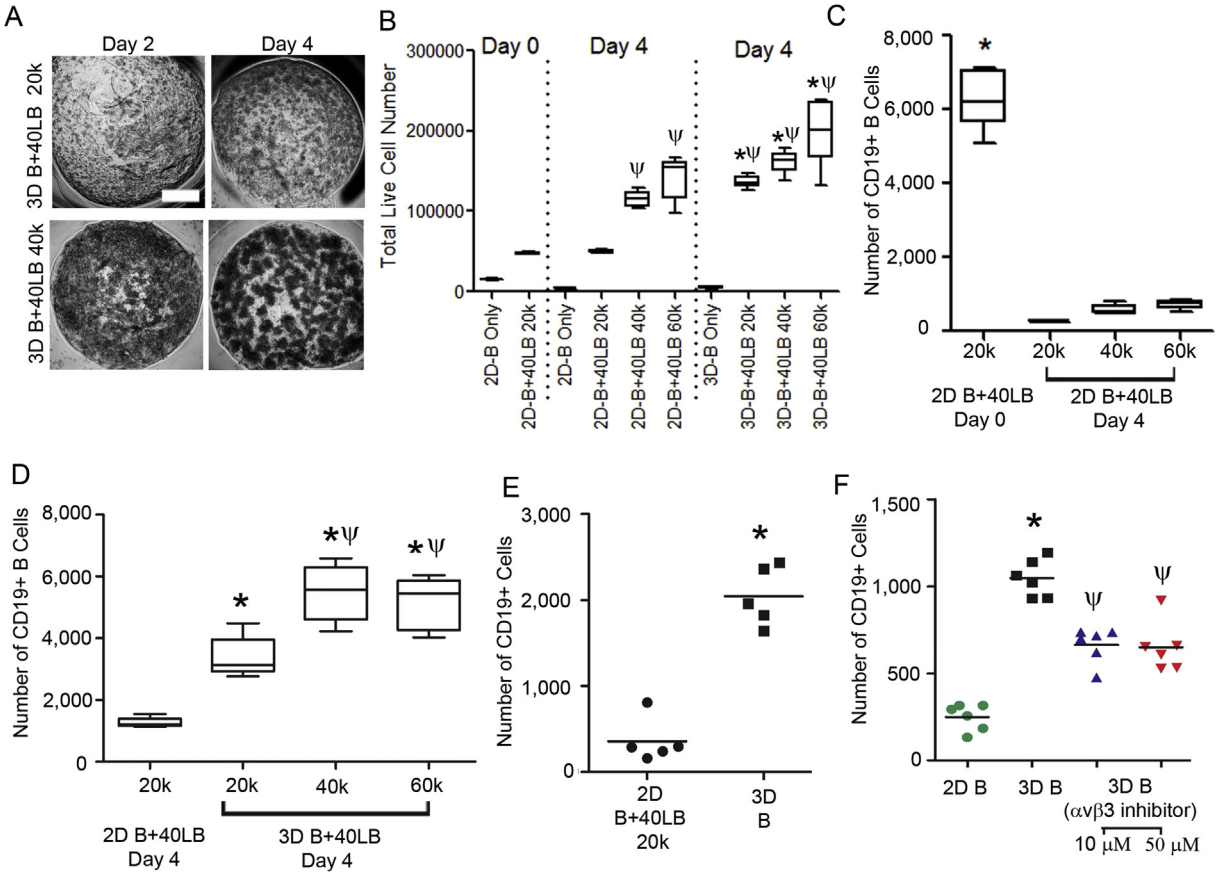

Fig. 4. *Ex vivo* proliferation of primary B cells within the immune organoid and role of integrins. (A) Phase images representing B cell proliferation within the organoids with varying number of stromal cells as a function of time. Scale bar: 500 μm. (B) Total number of viable cells on day 0 and 4. Box-whisker plot, *P < 0.05 w.r.t 2D groups on day 4 and ΨP < 0.05 w.r.t day 0, 1-way ANOVA with post-hoc Tukey's correction. (C, D) Fold expansion plot of CD19+ cells in different matrix architectures (2D vs. 3D) and various 40LB cell amounts (20,000, 40,000, and 60,000) after 6 days in culture (Box-whisker plot, n = 5). Each hydrogel (10 μL) consisted of 20,000 naïve B cells and at the completion of study, harvested cells from each hydrogel were equally divided into 3 groups for analysis. *P < 0.05 w.r.t 2D groups and ΨP < 0.05 w.r.t 3D with 20,000 40LBs, 2-way ANOVA with post-hoc Bonferroni correction. (E) Number of CD19+ cells in 2D co-cultures with 40LB (n = 5) and 3D organoids with no 40LB *P < 0.05, t-test. (F) Number of CD19+ cells in 2D versus 3D systems after 2 days in the presence or absence of 10 or 50 μM Cilengitide (Mean ± S.E.M, n = 5). *P < 0.05 w.r.t 2D groups and ΨP < 0.05 w.r.t 3D without Cilengitide, t-test.

increase in 2D B+40LB co-culture (Fig. 5A, Supplementary Fig. S2A). Within the 3D organoid cultures, the CD19+GL7+ response was dependent on 40LB seeding density where organoids with 40,000 40LB induced 96 ± 8 fold increase in CD19+GL7+ cell numbers that was significantly higher than 20,000 40LB group that induced 57 ± 5 fold increase ($p < 0.001$). There was no significant difference between 40,000 and 60,000 40LBs seeded organoids. These results were further confirmed by confocal studies that clearly demonstrate co-localization of GL7+ B cells on 40LB stromal network (Fig. 5B). We next examined whether SiNPs alone and gelatin organoids without nanoparticles using methacrylated gelatin (GelMA) could induce GC phenotype. GelMA is widely used in tissue engineering applications [56–58]. As indicated in Fig. 5C, SiNP alone or GelMA failed to induce activation of GL7+ cells. In contrast, Gelatin-SiNP organoids induced significant generation of GC phenotype. These results emphasize the importance of 3D organoid and presence of SiNP in the organoids for efficient GC reaction. Since expression of Fas ligand (CD95) is a hallmark of GC B cells and critical for their clonal selection, we examined the expression profile of Fas within the CD19+GL7+ cell population in the organoids and compared to the 2D co-cultures of B+40LB. As indicated in Fig. 5D and Supplementary Fig. S2B, immune organoids with 40,000 and 60,000 40LB cells demonstrated a significant 55-fold increase in CD19+GL7+Fas+ GC B cells compared to 2D B+40LB (7 ± 1 fold) and 3D B+40LB co-cultures at 20,000 40LB cell density (16 ± 2 fold). Despite the B cell proliferation, organoids with no stromal cells failed to induce GC B cell phenotype.

3.5. Antibody isotype class switching in the immune organoid

Another hallmark of GC reaction is the antibody class switching that occurs in GC B cells to produce antibodies with distinct effector functions [59–61]. Activated B cells are known to undergo antibody class switching from IgM to IgG or other Igs. Recognizing that the 3D immune organotypic cultures induced a phenotypic GC reaction, we then tested its functionality by analyzing antibody class-switching from IgM to IgG1 and IgE compared. Using flow cytometry on cells extracted from the organoids, we observed a robust class switching where the number of IgG1+ B cells increased

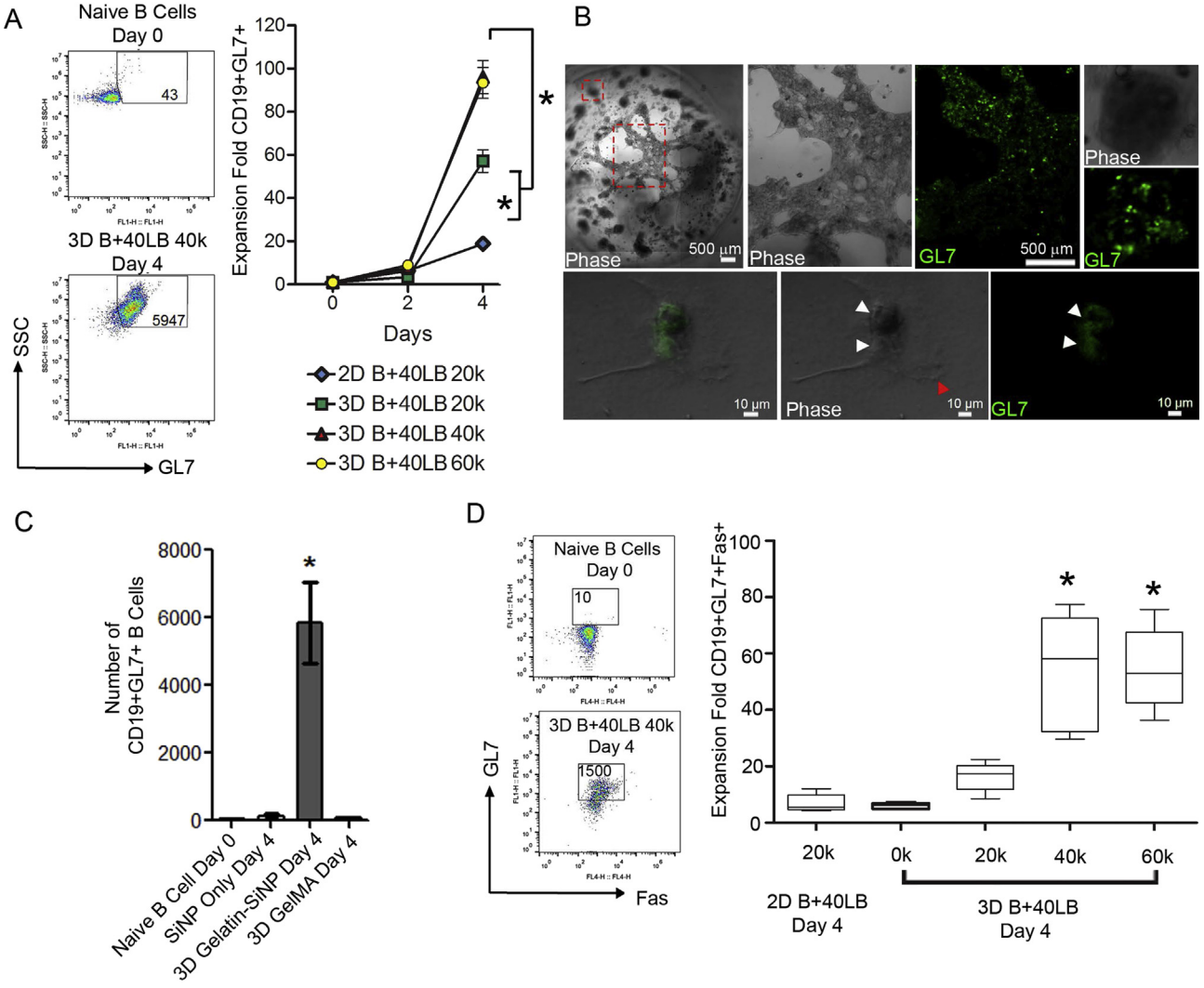

Fig. 5. *Ex vivo* induction into GC reaction within the immune organoid. (A) Fold increase in GC B cells (CD19+GL7+) after 4 days in culture (Mean ± S.E.M, n = 5). Approximately fifty CD19+GL7+ cells were detected in naïve B cell population on day 0. Left panel represents scatter plot from flow cytometry with numbers indicating the GL7+ cells. *$P < 0.05$, 2-way ANOVA with post-hoc Bonferroni correction. (B) Immunofluorescence analysis of GC B cells (CD19+GL7+) in the presence of 40LB stromal cells inside the organoid. (C) Number of CD19+ GL7+ GC B cells on day 4 after encapsulation in organoids of gelatin-SiNP or GelMA or cultured in 2D with SiNP (Bottom Panel, Mean ± S.E.M, n = 5). *$P < 0.05$, ANOVA with post-hoc Tukey's test. (D) Gating strategy for GC phenotype analysis where CD19+ B cells were double stained with GL7 and Fas (Left Panel). Fold increase in the number CD19+ GL7+ Fas+ GC B cells on day 4 after encapsulation in organoids or cultured in 2D (Right Panel, Box-whisker plot, n = 5). *$P < 0.05$, ANOVA with post-hoc Tukey's test.

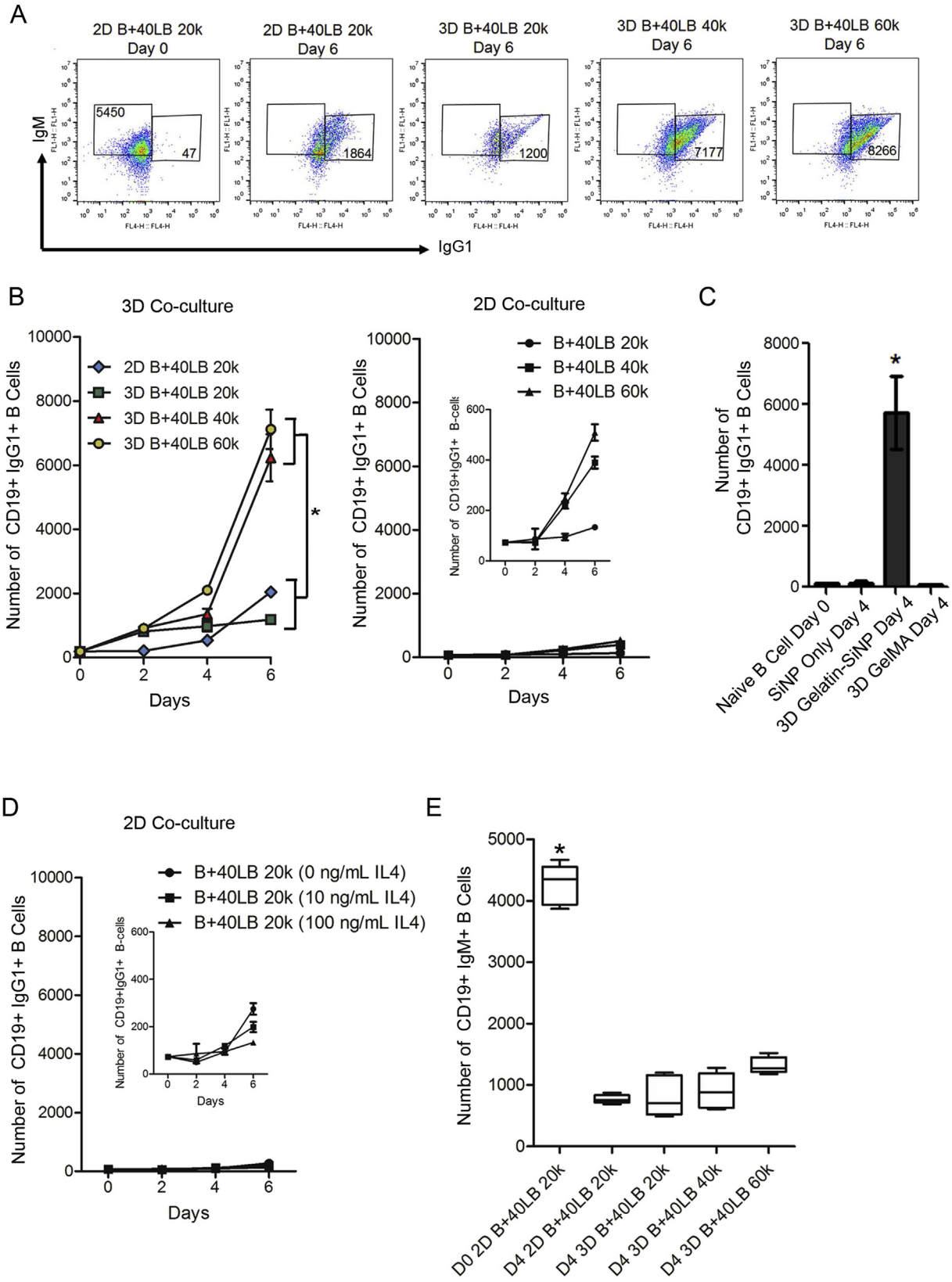

Fig. 6. Antibody isotype class switching in the immune organoid. (A) Gating strategy for GC phenotype analysis where CD19+ B cells were double stained with IgM and IgG1. Naïve B cells on day 0 predominantly express IgM and no IgG1. (B) Increase in the number of CD19+IgG1+ B cells over 6 days in 3D immune organoids or 2D co-cultures. *P < 0.05, 2-way ANOVA with post-hoc Bonferroni correction. (C) Number of CD19+ IgG1+ GC B cells on day 4 after encapsulation in organoids of gelatin-SiNP or GelMA or cultured in 2D with SiNP (Bottom Panel, Mean ± S.E.M, n = 5). *P < 0.05, ANOVA with post-hoc Tukey's test. (D, E) Fold increase in the number CD19+IgG1+ B cells over 6 days in 2D culture. (D) Fold change for 2D B+40LB with 20,000 40LBs at 0, 10, and 100 ng/mL IL4. (C) fold change for 2D B+40LB with 20,000–60,000 40LBs at 100 ng/mL IL4; (Mean ± S.E.M, n = 5). (Mean ± S.E.M, n = 5, *P < 0.05, 2-way ANOVA with post-hoc Bonferroni correction) (E) Bar graph represents a decrease in the number of CD19+IgM+ B cells on day 4 after encapsulation in organoids or cultured in 2D (Box-whisker plot, n = 5). *P < 0.05, ANOVA with post-hoc Tukey's test.

significantly from 185 ± 14 cells on day 0 to 7120 ± 612 cells on day 6 in 3D B+40LB organoids with 40,000 40LB cells (Fig. 6A,B). The cell numbers observed in 3D B+40LB organoids with 40,000 40LB cells were comparable to 3D organoids with 60,000 40LB cells. No such increase in CD19+IgG1+ B cells was observed in 2D B+40LB cultures with 40,000 and 60,000 40LB cells (Fig. 6C) or with GelMA (Fig. 6C) or with increasing concentration of IL-4 (Fig. 6D). The number of CD19+IgM+ B cells decreased significantly across all groups compared to day 0 (Fig. 6E). We next examined the levels of membrane-bound IgE expression and as indicated in Fig. 7, observed a marked shift in the mean fluorescence intensity of CD19+IgE+ cells in 3D groups with higher 40LB seeding density on day 6 compared to 2D B+40LB on day 6 and naïve B cells on day 0. Comparative analysis demonstrated a significant increase in the CD19+IgE+ level with 3D B+40LB organoids containing 40,000 40LBs (5446 ± 536 cells) and 60,000 40LBs (4441 ± 510 cells) as compared to 1687 ± 116 cells observed with 2D B+40LB co-cultures (Fig. 7).

4. Discussion

Engineered *ex vivo* tissues for culturing primary immune cells and allowing them to interact with their microenvironment could be a powerful strategy to understand and manipulate immune cell behavior. However, very few studies have been done in this area. Current design rationale behind tissue engineered secondary lymphoid organ is inspired from the mechanically soft nature of the lymphoid microenvironment and the presence of key cell signaling molecules, as well as the organogenesis and plasticity of which has been discussed by Irvine et al. [39]. However, till date, no modular *ex vivo* B cell follicle has been developed with an ability to accelerate immune reactions through tunable design parameters. In this paper we describe the development of a highly effective 3D B cell organoids that phenotypically and functionally resemble the GC reaction in a secondary lymphoid tissue. The design of the immune organoid was based on structural, mechanical, and cellular composition of the secondary lymphoid organs. In our studies, stromal 40LB cells demonstrated enhanced spreading and network formation when cultured in matrices with ~2000 Pa storage modulus and as a function of stromal cell density. This stiffness is closer to previously reported lymphoid tissue stiffness [52]. These findings explain a mechanism by which organoids support spreading of 40LBs which enables better cell–cell contact between stromal and B cells leading to superior B cell proliferation and activation.

An important finding of this study is that compared to 2D co-cultures, 3D immune organoids resulted in ~100-fold higher and rapid differentiation of naïve primary B cells to the GC phenotype with robust antibody class switching. Although prior studies have shown the critical role of CD40 signaling in 2D cultures, our findings indicate that αvβ3 integrin helps with GC B cell survival in the organoids and yet CD40L is critical for induction of GC phenotype. The αvβ3 integrin findings are consistent with the known role of αvβ3 in GC B cell fitness, *in vivo* [41]. In addition, SiNP appear to be critical for GC reaction because GelMA with B+40LB failed to induce GC phenotype. To further confirm the role of 3D ECM, stromal cell signaling and IL-4 in our observations, 2D B+40LB cultures were examined at 0, 10, and 100 ng/mL IL-4 and across 20,000–60,000 40LB seeding density. As expected, 2D cultures failed to efficiently induce the activation markers CD19+GL7+Fas+ across 0–100 ng/mL IL-4 (Supplementary Fig. S3). At 100 ng/mL, increasing 40LB density to 40,000 and 60,000 cells resulted in a maximum of 20-fold appearance of GL7+Fas+ B cells, which was significantly lower than those observed with 3D cultures (55 ± 6 fold, $p < 0.001$, Supplementary Fig. S3). These findings indicate that ECM, SiNP, and stromal signaling are critical for induction of the GC phenotype in naïve B cells cultured in 3D organoids. While the current study demonstrates the role of αvβ3 integrins as a pro-survival signal to B cells, we cannot rule out the role of other integrin types presented gelatin matrix. Future investigations will focus on possible role of integrins α5β1, α4β1, and whether presence of nanoparticles leads to additive effect in induction of GC-response. The silicate nanoparticles used in this study to complex with gelatin are ultrathin nanomaterials, with a high degree of anisotropy and functionality [62]. These two dimensional nanoparticles exhibit great potential in the field of regenerative medicine and drug delivery as they interact with biological entities in a substantially different manner than their respective 3D nano-counter parts because of their high surface to volume ratio [63,64]. Synthetic silicates (such as $Na^{+}_{0.7}[(Mg_{5.5}Li_{0.3})Si_8O_{20}(OH)_4]^{-}_{0.7}$ used in this study) dissociate into nontoxic products (Na^{+}, Mg^{2+}, $Si(OH)_4$, Li^{+}) in aqueous conditions. Mg^{2+} plays a significant role in cellular adhesion via integrins [65,66]. Lithium activates Wnt-responsive genes by inhibiting the glycogen synthase kinase-3[beta] activity via

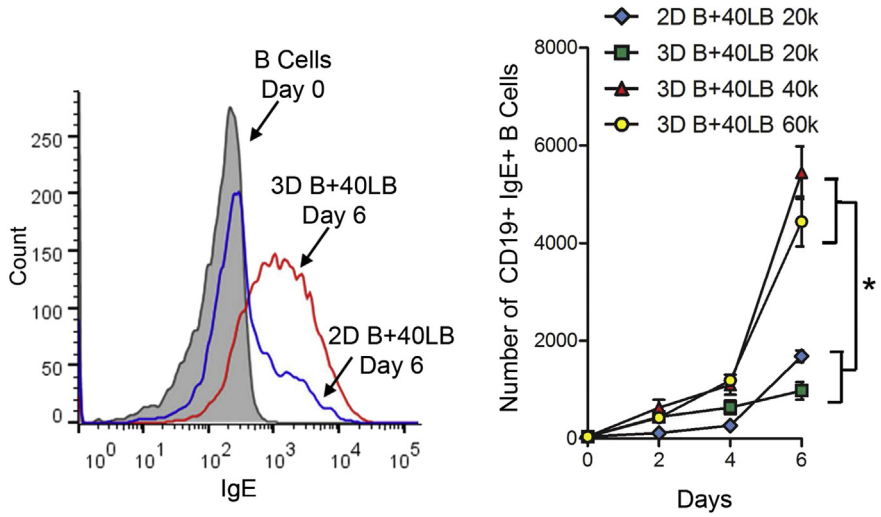

Fig. 7. IgE antibody expression in the immune organoid. Histogram representing the overlay of IgE expression for 2D and 3D co-cultures (Left). Increase in the number of CD19+IgE+ B cells over 6 days in 3D immune organoids or 2D co-cultures (total 30–40 CD19+IgE+ B cells on day 0). (Mean ± S.E.M, n = 5, *P < 0.05, 2-way ANOVA with post-hoc Bonferroni correction).

regulating Runt-related transcription factor-2 (RUNX2) activity. Role of Wnt signaling has been implicated in survival of GC B cells [67]. We further confirmed that the observed effect was specific to the organoids and not any bacterial endotoxins. Observations from LAL assay indicate 0.01 ± 0.001 endotoxin units (EU)/mL for SiNP alone and 0.04 ± 0.01 EU/mL for gelatin-SiNP organoids, which are below the US FDA threshold of 0.5 EU/mL.

In conclusion, our secondary follicle organoid provides a simple strategy for recapitulating the functional aspects of a lymphoid tissue to induce accelerated GC reaction *ex vivo* with maintained long-term cell survival by simply adjusting the extracellular signal. This approach can be distinguished from conventional GC induction protocols that rely on either culturing B cells as a 2D monolayer on tissue culture dishes in the presence of key molecules or transplantation of cell-seeded scaffold into live animal models for organoid formation *in vivo*. We anticipate that the ability to drive GC reaction *ex vivo* at controllable rates grants us the ability to reproduce immunological events with tunable parameters for better screening and translation of immunotherapeutics and other biotechnology avenues. Our natural gene rearrangement processes (somatic hypermutation and antibody class switching) are hallmark of antibody response to infections however could simultaneously lead to changes in a few genes involved in apoptosis and stress protection mechanism eventually leading to lymphoma in germinal centers. Therefore, biomaterials-based *ex vivo* immune organoids could further represent a new approach to study GC pathogenesis as in case of B cell malignancies [15] and for rational screening of biotherapeutics against such malignancies.

Author contributions

A.P. conducted all experiments, collected data and performed data analysis. M.A and A.G. performed SEM and mechanical testing experiments; T.N. and D.K. generated the 40LB cells; H.A performed immunohistochemistry and L.C contributed to the experimental design. A.S developed the concept, and together with A.P. contributed to the planning and design of the project. A.P. and A.S wrote the manuscript and all authors discussed the results and commented on the manuscript.

Acknowledgments

The authors acknowledge financial support from the National Institutes of Health (1R21CA185236-01), the Cornell University and Weill Cornell Medical College seed grant program, and the Howard Hughes Medical Institute (HHMI 56006761). The authors also thank C. Hernandez, A. August, and R. Weiss at Cornell University for providing animal tissues. The content is solely the responsibility of the authors and does not necessarily represent the official views of the funding agencies.

Appendix A. Supplementary data

Supplementary data related to this article can be found at http://dx.doi.org/10.1016/j.biomaterials.2015.06.002.

References

[1] M. McHeyzer-Williams, S. Okitsu, N. Wang, L. McHeyzer-Williams, Molecular programming of B cell memory, Nat. Rev. Immunol. 12 (2012) 24–34.
[2] C. Berek, A. Berger, M. Apel, Maturation of the immune response in germinal centers, Cell 67 (1991) 1121–1129.
[3] A. Singh, N.A. Peppas, Hydrogels and scaffolds for immunomodulation, Adv. Mater. 26 (2014) 6530–6541.
[4] T. Junt, E. Scandella, B. Ludewig, Form follows function: lymphoid tissue microarchitecture in antimicrobial immune defence, Nat. Rev. Immunol. 8 (2008) 764–775.
[5] G. Magri, M. Miyajima, S. Bascones, A. Mortha, I. Puga, L. Cassis, et al., Innate lymphoid cells integrate stromal and immunological signals to enhance antibody production by splenic marginal zone B cells, Nat. Immunol. 15 (2014) 354–364.
[6] A. Cerutti, M. Cols, I. Puga, Marginal zone B cells: virtues of innate-like antibody-producing lymphocytes, Nat. Rev. Immunol. 13 (2013) 118–132.
[7] P. Zhou, D.R. Shaffer, D.A. Alvarez Arias, Y. Nakazaki, W. Pos, A.J. Torres, et al., In vivo discovery of immunotherapy targets in the tumour microenvironment, Nature 506 (2014) 52–57.
[8] T.A. Schwickert, R.L. Lindquist, G. Shakhar, G. Livshits, D. Skokos, M.H. Kosco-Vilbois, et al., In vivo imaging of germinal centres reveals a dynamic open structure, Nature 446 (2007) 83–87.
[9] C.D. Allen, K.M. Ansel, C. Low, R. Lesley, H. Tamamura, N. Fujii, et al., Germinal center dark and light zone organization is mediated by CXCR4 and CXCR5, Nat. Immunol. 5 (2004) 943–952.
[10] L.C. Cerchietti, K. Hatzi, E. Caldas-Lopes, S.N. Yang, M.E. Figueroa, R.D. Morin, et al., BCL6 repression of EP300 in human diffuse large B cell lymphoma cells provides a basis for rational combinatorial therapy, J. Clin. Invest. 120 (2010) 4569–4582.
[11] L.C. Cerchietti, A.F. Ghetu, X. Zhu, G.F. Da Silva, S. Zhong, M. Matthews, et al., A small-molecule inhibitor of BCL6 kills DLBCL cells in vitro and in vivo, Cancer Cell. 17 (2010) 400–411.
[12] U. Klein, R. Dalla-Favera, Germinal centres: role in B-cell physiology and malignancy, Nat. Rev. Immunol. 8 (2008) 22–33.
[13] P. Ame-Thomas, J. Le Priol, H. Yssel, G. Caron, C. Pangault, R. Jean, et al., Characterization of intratumoral follicular helper T cells in follicular lymphoma: role in the survival of malignant B cells, Leukemia 26 (2012) 1053–1063.
[14] G. Lenz, G. Wright, S.S. Dave, W. Xiao, J. Powell, H. Zhao, et al., Stromal gene signatures in large-B-cell lymphomas, N. Engl. J. Med. 359 (2008) 2313–2323.
[15] F. Cayrol, M.C. Diaz Flaque, T. Fernando, S.N. Yang, H.A. Sterle, M. Bolontrade, et al., Integrin alphavbeta3 acting as membrane receptor for thyroid hormones mediates angiogenesis in malignant T cells, Blood 125 (2015) 841–851.
[16] T. Clozel, S. Yang, R. Elstrom, W. Tam, P. Martin, M. Kormaksson, S. Banerjee, A. Vasanthakumar, B. Culjkovic, D. Scott, S. Brennan, M. Leser, R. Shaknovich, A. Chadburn, F. Tabbo, L. Godley, R. Gascoyne, K. Borden, G. Inghirami, J. Leonard, A. Melnick, L. Cerchietti, Mechanism-based epigenetic chemosensitization therapy of diffuse large B Cell Lymphoma, Cancer Discov. 3 (2013) 1002–1019.
[17] S. De, R. Shaknovich, M. Riester, O. Elemento, H. Geng, M. Kormaksson, et al., Aberration in DNA methylation in B-cell lymphomas has a complex origin and increases with disease severity, PLoS Genet. 9 (2013) e1003137.
[18] L. Fontan, C. Yang, V. Kabaleeswaran, L. Volpon, M.J. Osborne, E. Beltran, et al., MALT1 small molecule inhibitors specifically suppress ABC-DLBCL in vitro and in vivo, Cancer Cell. 22 (2012) 812–824.
[19] L.C. Cerchietti, S.N. Yang, R. Shaknovich, K. Hatzi, J.M. Polo, A. Chadburn, et al., A peptomimetic inhibitor of BCL6 with potent antilymphoma effects in vitro and in vivo, Blood 113 (2009) 3397–3405.
[20] L.C. Cerchietti, E.C. Lopes, S.N. Yang, K. Hatzi, K.L. Bunting, L.A. Tsikitas, et al., A purine scaffold Hsp90 inhibitor destabilizes BCL-6 and has specific antitumor activity in BCL-6-dependent B cell lymphomas, Nat. Med. 15 (2009) 1369–1376.
[21] L.C. Cerchietti, J.M. Polo, G.F. Da Silva, P. Farinha, R. Shaknovich, R.D. Gascoyne, et al., Sequential transcription factor targeting for diffuse large B-cell lymphomas, Cancer Res. 68 (2008) 3361–3369.
[22] J.M. Polo, T. Dell'Oso, S.M. Ranuncolo, L. Cerchietti, D. Beck, G.F. Da Silva, et al., Specific peptide interference reveals BCL6 transcriptional and oncogenic mechanisms in B-cell lymphoma cells, Nat. Med. 10 (2004) 1329–1335.
[23] A. Singh, H. Qin, I. Fernandez, J. Wei, J. Lin, L.W. Kwak, et al., An injectable synthetic immune-priming center mediates efficient T-cell class switching and T-helper 1 response against B cell lymphoma, J. Control. Release: Off. J. Control. Release Soc. 155 (2011) 184–192.
[24] H. Qin, S.C. Cha, S.S. Neelapu, Y. Lou, J. Wei, Y.J. Liu, et al., Vaccine site inflammation potentiates idiotype DNA vaccine-induced therapeutic T cell-, and not B cell-, dependent antilymphoma immunity, Blood 114 (2009) 4142–4149.
[25] R. Chiarle, W.J. Simmons, H. Cai, G. Dhall, A. Zamo, R. Raz, et al., Stat3 is required for ALK-mediated lymphomagenesis and provides a possible therapeutic target, Nat. Med. 11 (2005) 623–629.
[26] R. Chiarle, J.Z. Gong, I. Guasparri, A. Pesci, J. Cai, J. Liu, et al., NPM-ALK transgenic mice spontaneously develop T-cell lymphomas and plasma cell tumors, Blood 101 (2003) 1919–1927.
[27] A. Singh, S. Suri, K. Roy, In-situ crosslinking hydrogels for combinatorial delivery of chemokines and siRNA-DNA carrying microparticles to dendritic cells, Biomaterials 30 (2009) 5187–5200.
[28] A. Singh, H. Nie, B. Ghosn, H. Qin, L.W. Kwak, K. Roy, Efficient modulation of T-cell response by dual-mode, single-carrier delivery of cytokine-targeted siRNA and DNA vaccine to antigen-presenting cells, Mol. Ther. 16 (2008) 2011–2021.
[29] A. Purwada, K. Roy, A. Singh, Engineering vaccines and niches for immune modulation, Acta Biomater. 10 (2013) 1728–1740.
[30] B. Schiemann, J.L. Gommerman, K. Vora, T.G. Cachero, S. Shulga-Morskaya, M. Dobles, et al., An essential role for BAFF in the normal development of B cells through a BCMA-independent pathway, Science 293 (2001) 2111–2114.

[31] B.A. Heesters, R.C. Myers, M.C. Carroll, Follicular dendritic cells: dynamic antigen libraries, Nat. Rev. Immunol. 14 (2014) 495–504.
[32] J. Song, Z. Lokmic, T. Lämmermann, J. Rolf, C. Wu, X. Zhang, et al., Extracellular matrix of secondary lymphoid organs impacts on B-cell fate and survival, Proc. Natl. Acad. Sci. 110 (2013) E2915–E2924.
[33] Y.J. Liu, D.E. Joshua, G.T. Williams, C.A. Smith, J. Gordon, I.C. MacLennan, Mechanism of antigen-driven selection in germinal centres, Nature 342 (1989) 929–931.
[34] H. Martinez-Valdez, C. Guret, O. de Bouteiller, I. Fugier, J. Banchereau, Y.J. Liu, Human germinal center B cells express the apoptosis-inducing genes Fas, c-myc, P53, and Bax but not the survival gene bcl-2, J. Exp. Med. 183 (1996) 971–977.
[35] A. Cerutti, H. Zan, A. Schaffer, L. Bergsagel, N. Harindranath, E.E. Max, et al., CD40 ligand and appropriate cytokines induce switching to IgG, IgA, and IgE and coordinated germinal center and plasmacytoid phenotypic differentiation in a human monoclonal IgM+ IgD+ B cell line, J. Immunol. 160 (1998) 2145–2157.
[36] M.S. von Bergwelt-Baildon, R.H. Vonderheide, B. Maecker, N. Hirano, K.S. Anderson, M.O. Butler, et al., Human primary and memory cytotoxic T lymphocyte responses are efficiently induced by means of CD40-activated B cells as antigen-presenting cells: potential for clinical application, Blood 99 (2002) 3319–3325.
[37] J.L. Schultze, S. Michalak, M.J. Seamon, G. Dranoff, K. Jung, J. Daley, et al., CD40-activated human B cells: an alternative source of highly efficient antigen presenting cells to generate autologous antigen-specific T cells for adoptive immunotherapy, J. Clin. Invest. 100 (1997) 2757.
[38] C.M. Coughlin, B.A. Vance, S.A. Grupp, R.H. Vonderheide, RNA-transfected CD40-activated B cells induce functional T-cell responses against viral and tumor antigen targets: implications for pediatric immunotherapy, Blood 103 (2004) 2046–2054.
[39] D.J. Irvine, A.N. Stachowiak, Y. Hori, Lymphoid tissue engineering: invoking lymphoid tissue neogenesis in immunotherapy and models of immunity, Seminars Immunol. 20 (2008) 137–146.
[40] S. Suematsu, T. Watanabe, Generation of a synthetic lymphoid tissue-like organoid in mice, Nat. Biotechnol. 22 (2004) 1539–1545.
[41] X. Wang, L.B. Rodda, O. Bannard, J.G. Cyster, Integrin-mediated interactions between B cells and follicular dendritic cells influence germinal center B cell fitness, J. Immunol. 192 (2014) 4601–4609.
[42] K. Hatzi, Y. Jiang, C. Huang, F. Garrett-Bakelman, M.D. Gearhart, E.G. Giannopoulou, et al., A hybrid mechanism of action for BCL6 in B cells defined by formation of functionally distinct complexes at enhancers and promoters, Cell. Reports 4 (2013) 578–588.
[43] T. Murakami, X. Chen, K. Hase, A. Sakamoto, C. Nishigaki, H. Ohno, Splenic CD19-CD35+B220+ cells function as an inducer of follicular dendritic cell network formation, Blood 110 (2007) 1215–1224.
[44] R.C. Rickert, K. Rajewsky, J. Roes, Impairment of T-cell-dependent B-cell responses and B-1 cell development in CD19-deficient mice, Nature 376 (1995) 352–355.
[45] T. Nojima, K. Haniuda, T. Moutai, M. Matsudaira, S. Mizokawa, I. Shiratori, et al., In-vitro derived germinal centre B cells differentially generate memory B or plasma cells in vivo, Nat. Commun. 2 (2011) 465.
[46] M.B. Gorbet, M.V. Sefton, Endotoxin: the uninvited guest, Biomaterials 26 (2005) 6811–6817.
[47] A. Dolatshahi-Pirouz, M. Nikkhah, A.K. Gaharwar, B. Hashmi, E. Guermani, H. Aliabadi, et al., A combinatorial cell-laden gel microarray for inducing osteogenic differentiation of human mesenchymal stem cells, Sci. Rep. 4 (2014) 3896.
[48] R.G. Patel, A. Purwada, L. Cerchietti, G. Inghirami, A. Melnick, A.K. Gaharwar, et al., Microscale bioadhesive hydrogel arrays for cell engineering applications, Cell. Mol. Bioeng. 7 (2014) 394–408.
[49] A.K. Gaharwar, R.K. Avery, A. Assmann, A. Paul, G.H. McKinley, A. Khademhosseini, et al., Shear-thinning nanocomposite hydrogels for the treatment of hemorrhage, ACS Nano 8 (2014) 9833–9842.
[50] J.R. Xavier, T. Thakur, P. Desai, M.K. Jaiswal, N. Sears, E. Cosgriff-Hernandez, et al., Bioactive nanoengineered hydrogels for bone tissue engineering: a growth-factor-free approach, ACS Nano 9 (2015) 3109–3118.
[51] T. Fujita, M. Kashimura, Scanning electron microscope studies of human spleen, Surv. Immunol. Res. 2 (1983) 375–384.
[52] S. Hirsch, J. Guo, R. Reiter, S. Papazoglou, T. Kroencke, J. Braun, et al., MR elastography of the liver and the spleen using a piezoelectric driver, single-shot wave-field acquisition, and multifrequency dual parameter reconstruction, Magn. Reson Med. 71 (2014) 267–277.
[53] Q. Xing, K. Yates, C. Vogt, Z. Qian, M.C. Frost, F. Zhao, Increasing mechanical strength of gelatin hydrogels by divalent metal ion removal, Sci. Rep. 4 (2014) 4706.
[54] R. Stupp, M.E. Hegi, T. Gorlia, S.C. Erridge, J. Perry, Y.K. Hong, et al., Cilengitide combined with standard treatment for patients with newly diagnosed glioblastoma with methylated MGMT promoter (CENTRIC EORTC 26071-22072 study): a multicentre, randomised, open-label, phase 3 trial, Lancet Oncol. 15 (2014) 1100–1108.
[55] C. Mas-Moruno, F. Rechenmacher, H. Kessler, Cilengitide: the first anti-angiogenic small molecule drug candidate design, synthesis and clinical evaluation, Anticancer Agents Med. Chem. 10 (2010) 753–768.
[56] R.Z. Lin, Y.C. Chen, R. Moreno-Luna, A. Khademhosseini, J.M. Melero-Martin, Transdermal regulation of vascular network bioengineering using a photopolymerizable methacrylated gelatin hydrogel, Biomaterials 34 (2013) 6785–6796.
[57] J.A. Benton, C.A. DeForest, V. Vivekanandan, K.S. Anseth, Photocrosslinking of gelatin macromers to synthesize porous hydrogels that promote valvular interstitial cell function, Tissue Eng. Part A 15 (2009) 3221–3230.
[58] B. Duan, L.A. Hockaday, E. Kapetanovic, K.H. Kang, J.T. Butcher, Stiffness and adhesivity control aortic valve interstitial cell behavior within hyaluronic acid based hydrogels, Acta Biomater. 9 (2013) 7640–7650.
[59] B.Q. Vuong, M. Lee, S. Kabir, C. Irimia, S. Macchiarulo, G.S. McKnight, et al., Specific recruitment of protein kinase A to the immunoglobulin locus regulates class-switch recombination, Nat. Immunol. 10 (2009) 420–426.
[60] R. Shinkura, S. Ito, N.A. Begum, H. Nagaoka, M. Muramatsu, K. Kinoshita, et al., Separate domains of AID are required for somatic hypermutation and class-switch recombination, Nat. Immunol. 5 (2004) 707–712.
[61] N. Liu, N. Ohnishi, L. Ni, S. Akira, K.B. Bacon, CpG directly induces T-bet expression and inhibits IgG1 and IgE switching in B cells, Nat. Immunol. 4 (2003) 687–693.
[62] B. Ruzicka, E. Zaccarelli, L. Zulian, R. Angelini, M. Sztucki, A. Moussaid, et al., Observation of empty liquids and equilibrium gels in a colloidal clay, Nat. Mater. 10 (2011) 56–60.
[63] A.K. Gaharwar, N.A. Peppas, A. Khademhosseini, Nanocomposite hydrogels for biomedical applications, Biotechnol. Bioeng. 111 (2014) 441–453.
[64] P. Kerativitayanan, J.K. Carrow, A.K. Gaharwar, Nanomaterials for engineering stem cell responses, Adv. Healthc. Mater. (2015), http://dx.doi.org/10.1002/adhm.201500272.
[65] D.F. Legler, G. Wiedle, F.P. Ross, B.A. Imhof, Superactivation of integrin alphavbeta3 by low antagonist concentrations, J. Cell. Sci. 114 (2001) 1545–1553.
[66] T. Kinashi, Intracellular signalling controlling integrin activation in lymphocytes, Nat. Rev. Immunol. 5 (2005) 546–559.
[67] J. Kim, D.W. Kim, W. Chang, J. Choe, C.S. Park, K. Song, et al., Wnt5a is secreted by follicular dendritic cells to protect germinal center B cells via Wnt/Ca2+/NFAT/NF-kappaB-B cell lymphoma 6 signaling, J. Immunol. 188 (2012) 182–189.